End-Effector Contact Force Estimation for Aerial Manipulators

Bredenbeck, A.; Della Santina, C.; Hamaza, S.

Important note
To cite this publication, please use the final published version (if applicable).
Please check the document version above.

End-Effector Contact Force Estimation for Aerial Manipulators

Anton Bredenbeck[1], Cosimo Della Santina[2], Salua Hamaza[1]

{a.bredenbeck c.dellasantina s.hamaza}@tudelft.nl

Abstract— Unmanned Aerial Vehicles (UAVs) are widely used for environmental surveying and exploration thanks to their maneuverability and accessibility. Until recently, however, these platforms were mainly used as passive systems that observe their environments visually and do not interact physically. The capability of UAVs to physically interact with their environment, also known as Aerial Manipulators (AMs), allows them to do a wider variety of tasks. These tasks include contact inspection, manipulation of objects, and more.

To successfully interact with the environment, the AM must compensate for the contact-induced disturbance forces. One approach is to estimate the contact force and compensate for it within the control approach.

This work introduces a framework to estimate the contact force at the End-Effector (EE) using only state measurements of the generic AM. Further, the evaluation of the framework in a simulation of an AM with a tendon-driven robotic arm shows that it precisely estimates the contact force.

I. INTRODUCTION

UAVs are a popular solution for environmental surveying in various applications. Combined with visual sensors, they are highly agile [1] and provide a broad spectrum of information ranging from agricultural crop information to structural integrity of infrastructure [2].

While UAVs excel in the domain of visual surveying and observation, their interacting counterparts – the AMs – have only recently started to achieve promising results in literature [3]–[6]. The above examples successfully conduct interaction tasks such as accurate EE positioning, contour following, and contact-based inspection. The mentioned works have in common that they directly measure the contact force. The measured force then functions as an input to a direct or indirect force controller, depending on the task. In the case of direct force control, the sensors are in place for groundtruthing. However, they are delicate and costly sensing devices unsuitable for low-cost solutions.

An alternative way to estimate the contact force is to employ a robotic arm with measurable stiffness at the joints. The robotic arm will attain a known posture given some control input and known external forces – such as gravity. Under the influence of an unknown external force, measuring the joint positions and velocities results in a disparity from that known posture. If one assumes the location of contact is known, the magnitude and direction of the external force are a direct function of the abovementioned measurements. They thus can be inferred without directly measuring them.
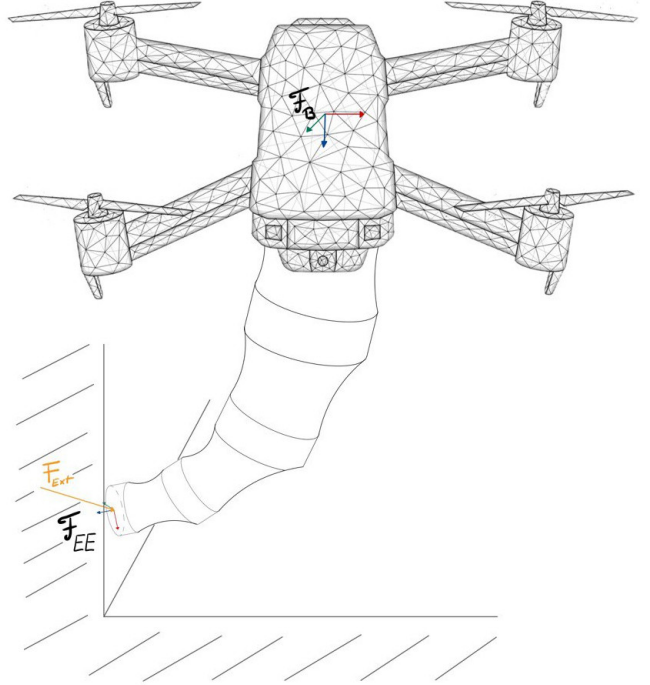

Fig. 1: A UAV equipped with a compliant finger in contact with its surroundings. From measuring the manipulator state the contact force can be estimated and used for force control to maintain contact with the environment.

This work showcases this approach to contact force estimation for a generic AM. We further evaluate it, in simulation, on a more concrete example. To enable a lightweight design in the future, we model the robotic arm as rigid links connected by universal joints driven by a tendon.

The rest of this letter is structured as follows: next, we introduce the mathematical model of the overall system in section II, followed by the derivation for the contact force in the dynamic and static case in section III. We further introduce the simulation used for validation in section IV, including the employed position controller, the contact model, and the scenario simulated. Finally, we show the results in section V and close with some concluding remarks in section VI.

II. MODELLING THE AERIAL MANIPULATOR

The overall system consists of a free-floating base and a soft, compliant arm. The free-floating system is described by the six Degrees-of-Freedom (DoFs) pose $\mathbf{x} = \begin{bmatrix} \mathbf{p} & \mathbf{\Omega} \end{bmatrix}^T \in \begin{bmatrix} \mathbb{R}^3 & \mathrm{SO}(3) \end{bmatrix}^T$ which contains the Euclidean coordinates of

[1]Biomorphic Intelligence Lab, Dept. of Control & Operations, Faculty of Aerospace Engineering, TU Delft

[2]Dept. of Cognitive Robotics, Faculty of Mech. Engineering, TU Delft

Variable	Definition
$\mathbf{M}_{Base}$	Mass-Inertia Matrix of the Base
$\mathbf{M}_{Arm}$	Mass-Inertia Matrix of the Arm
$\mathbf{H}$	Coupling Matrix between the Base and the Arm
$\mathbf{K}(\mathbf{q})$	Stiffness contribution of the Arm
$\mathbf{D}_{Base}$	Damping of the Base
$\mathbf{D}_{Arm}(\mathbf{q})$	Damping of the Arm
$\mathbf{C}_{Base}(\mathbf{q}, \dot{\mathbf{q}})$	Coriolis Contribution to the Base
$\mathbf{C}_{Arm}(\mathbf{q}, \dot{\mathbf{q}})$	Coriolis Contribution to the Arm
$\mathbf{G}_{B2B}$	Gravity Contribution to the Base by the Base
$\mathbf{G}_{A2B}$	Gravity Contribution to the Base by the Arm
$\mathbf{G}_{A2A}$	Gravity Contribution to the Arm by the Arm
$\mathbf{A}_{Base}$	Map of the rotor speeds to the generalized forces on the base
$\mathbf{A}_{Arm}$	Map of the tendon forces to the generalized forces on the arm joints.
$\mathbf{J}_{EE}(\mathbf{q})$	The EE Jacobian mapping state velocities ($\dot{\mathbf{q}}$) to EE velocites ($\mathbf{v}_{EE}$)
$\mathbf{f}_{Ext}$	The external force acting on the EE
τ_R	The forces enacted by the rotors
τ_T	The tendon tensions

the base's Center-of-Mass (CoM) ($\mathbf{p}$) as well as its attitude ($\mathbf{\Omega}$). Its derivative is denoted as $\mathbf{v} \in \mathbb{R}^6$ and contains the three linear velocities ($\dot{\mathbf{p}}$) and three angular velocities (ω). The compliant manipulator consists of n rigid links connected by n universal joints, i.e., joints with two rotational DoFs, where m tendons actuate the entire arm. Thus the arm's state is fully described by the state vector $\mathbf{q} \in \mathbb{R}^{2n}$, which packs the two DoFs of all joints.

Employing the standard Euler-Lagrange formalism, the equations of motion follow in the form of the standard manipulator equation [7]:

$$
\begin{aligned}
&\begin{bmatrix} \mathbf{M}_{Base} & \mathbf{H} \\ \mathbf{H}^T & \mathbf{M}_{Arm} \end{bmatrix} \begin{bmatrix} \dot{\mathbf{v}} \\ \ddot{\mathbf{q}} \end{bmatrix} + \begin{bmatrix} \mathbf{0} \\ \mathbf{K}(\mathbf{q}) \end{bmatrix} \\
&+ \begin{bmatrix} \mathbf{D}_{Base} & \mathbf{C}_{Base}(\mathbf{q}, \dot{\mathbf{q}}) \\ \mathbf{0} & \mathbf{D}_{Arm}(\mathbf{q}) + \mathbf{C}_{Arm}(\mathbf{q}, \dot{\mathbf{q}}) \end{bmatrix} \begin{bmatrix} \mathbf{v} \\ \dot{\mathbf{q}} \end{bmatrix} \\
&+ \begin{bmatrix} \mathbf{G}_{B2B} + \mathbf{G}_{A2B}(\mathbf{q}) \\ \mathbf{G}_{A2A}(\mathbf{q}) \end{bmatrix} \\
&= \mathbf{J}_{EE}^T(\mathbf{q})\mathbf{f}_{Ext} + \begin{bmatrix} \mathbf{A}_{Base} & \mathbf{0} \\ \mathbf{0} & \mathbf{A}_{Arm} \end{bmatrix} \begin{bmatrix} \tau_R \\ \tau_T \end{bmatrix} ,
\end{aligned} \tag{1}
$$

where all variables are defined in table I.

All terms contribute to the generalized forces acting on the system state. The first term expresses the system mass and inertia contribution, where the cross diagonal terms represent the dynamic coupling between the base and the manipulator. The second and third terms express the contribution of the stiffness of the arm and the gravity contribution. The two terms on the right side of the equation map the external force and control inputs to the generalized forces acting on the AM. Please refer to the linked repository for details on populating the matrices above.

III. CONTACT FORCE

Equation (1) provides a model for the behavior of the AM under the influence of actuation, gravity, and an unknown external force acting on the EE. Rearranging the equation yields the following expression for the external force:

$$
\begin{aligned}
\mathbf{f}_{External} = &\mathbf{J}_{EE}^T(\mathbf{q})^\dagger \Bigg(\begin{bmatrix} \mathbf{0} \\ \mathbf{K}(\mathbf{q}) \end{bmatrix} \\
&+ \begin{bmatrix} \mathbf{M}_{Base} & \mathbf{H} \\ \mathbf{H}^T & \mathbf{M}_{Arm} \end{bmatrix} \begin{bmatrix} \dot{\mathbf{v}} \\ \ddot{\mathbf{q}} \end{bmatrix} \\
&+ \begin{bmatrix} \mathbf{D}_{Base} & \mathbf{C}_{Base}(\mathbf{q}, \dot{\mathbf{q}}) \\ \mathbf{0} & \mathbf{D}_{Arm}(\mathbf{q}) + \mathbf{C}_{Arm}(\mathbf{q}, \dot{\mathbf{q}}) \end{bmatrix} \begin{bmatrix} \mathbf{v} \\ \dot{\mathbf{q}} \end{bmatrix} \\
&+ \begin{bmatrix} \mathbf{G}_{B2B} + \mathbf{G}_{A2B}(\mathbf{q}) \\ \mathbf{G}_{A2A}(\mathbf{q}) \end{bmatrix} \\
&- \begin{bmatrix} \mathbf{A}_{Base} & \mathbf{0} \\ \mathbf{0} & \mathbf{A}_{Arm} \end{bmatrix} \begin{bmatrix} \tau_R \\ \tau_T \end{bmatrix} \Bigg) ,
\end{aligned} \tag{2}
$$

where $[]^\dagger$ denotes the Moore-Penrose inverse [8]. If the system motion is assumed to be slow, the terms independent from the state velocity and acceleration dominate the dynamic equation. Hence, it follows that the mass-inertia contribution, the damping, and the Coriolis contribution are negligible with respect to all other components, i.e., the system becomes quasi-static. This implies that all system derivatives $\dot{\mathbf{v}}, \ddot{\mathbf{q}}, \mathbf{v}, \dot{\mathbf{q}}$ are equal to zero and therefore:

$$
\begin{aligned}
\mathbf{f}_{External,Static} = &\mathbf{J}_{EE}^T(\mathbf{q})^\dagger \Bigg(\begin{bmatrix} \mathbf{0} \\ \mathbf{K}(\mathbf{q}) \end{bmatrix} \\
&+ \begin{bmatrix} \mathbf{G}_{B2B} + \mathbf{G}_{A2B}(\mathbf{q}) \\ \mathbf{G}_{A2A}(\mathbf{q}) \end{bmatrix} \\
&- \begin{bmatrix} \mathbf{A}_{Base} & \mathbf{0} \\ \mathbf{0} & \mathbf{A}_{Arm} \end{bmatrix} \begin{bmatrix} \tau_R \\ \tau_T \end{bmatrix} \Bigg)
\end{aligned} \tag{3}
$$

IV. SIMULATION

For this analysis, we generate a planar model of the AM system, where a planar robotic arm is attached to the bottom of the aircraft. In the planar case, we assume that out-of-plane forces generated by the planar manipulator are negligible. Two tendons actuate the manipulator, and the overall system abides by the dynamic equation (1).

A. Bi-Rotor Control

For this work, we control the aircraft independently from the robotic arm. Figure 2a depicts the AM's dimensions. The controller takes the form of a classic multi-stage position controller, as depicted in figure 2b. With this, the controller computes a desired attitude $\mathbf{\Omega}$ given the planar components of some reference position. The controller then achieves the reference position using an LQR controller regulating the attitude, and an LQRi controller for the altitude.

B. Contact Model

Because of the discrete nature of simulation, simulating physical contact necessarily involves the contact objects penetrating each other. In that state, the simulation must then apply some force to act as a reaction force, bringing the objects out of penetration. In this work, we assume the contact to occur at a single point at the EE. The employed point contact model assumes a Spring-Damper
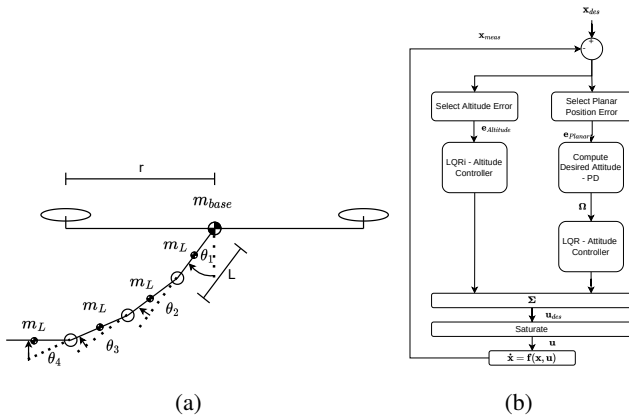
(a)   (b)

Fig. 2: Left: The physical properties of the model. Right: The base control architecture.
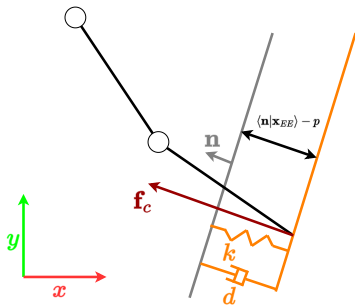

Fig. 3: The EE in penetration with a planar surface. The contact force $\mathbf{f}_c$ is modeled as a spring-damper system between the surface and the EE.

system between the object in penetration and the surface, characterized by its spring constant k and damping d [9]. Locally a surface can be approximated as a plane defined by its normal vector $\mathbf{n}$ and its distance parameter $p = \langle \mathbf{n} | \mathbf{v} \rangle$, where $\mathbf{v}$ is some point within the plane. The contact force $\mathbf{f}_c$ follows the geometric considerations from figure 3:

$$\mathbf{f}_c = [k\left(\langle \mathbf{n} | \mathbf{x}_{EE} \rangle - p\right) - d\left\langle \mathbf{n} | \dot{\mathbf{x}}_{EE} \right\rangle] \mathbf{n} , \tag{4}$$

which is non-zero whenever the condition

$$\langle \mathbf{n} | \mathbf{x}_{EE} \rangle - p \leq 0 \tag{5}$$

holds.

C. Study Case: Impact Against a Rigid Wall

In the simulated scenario the AM starts at the origin and is tasked with flying to a given location $(x = 3, y = 1)$ while enacting a constant force on one of the tendons ($\tau_{T,1} = 4\,\mathrm{N}$). This target location lies on the wall's surface, i.e., physically unreachable. During this flight, the EE makes contact with the unmovable wall (at $x = 3$), thus experiencing contact forces. Figure 2a shows a visualization of the model, and table II displays all physical parameters of the system.

V. RESULTS

Figures 4a and 4b show the trajectory of the AM system's base and the EE. The red force arrow indicates that the AM

TABLE II: AM physical parameters.

Property		
Mass	$m_{base} = 0.5\,\mathrm{kg}$	$m_{link} = 0.01\,\mathrm{kg}$
Length	$r_{base} = 0.1\,\mathrm{m}$	$l_{link} = 0.1\,\mathrm{m}$

successfully traverses towards the set-point and establishes contact at the EE. Further, considering the individual x-coordinate of the EE (cf. figure 4b), it exhibits a constant and minimal level of penetration with the contact surface after establishing contact. In particular, it doesn't exceed the wall coordinate ($x = 3$) by a significant amount, indicating that the simple contact model from subsection IV-B is sufficient.

Figure 4c displays the actual contact force, the dynamic estimation according to equation (2), where $\ddot{\mathbf{q}}$ is computed by numerically differentiating $\dot{\mathbf{q}}$, as well as the static estimation according to equation (3). The static and dynamic estimations both correctly estimate the contact force at the static equilibrium. However, the static estimation strongly diverges during flight and when establishing contact. This difference is anticipated since the static estimation neglects all dynamic effects, which are significant during the impact. The dynamic estimation follows the true contact force much closer. During the initial, very rapid maneuver, some noise occurs due to the approximation of numerically differentiating the velocities to obtain the acceleration. When establishing contact, the estimation initially overshoots the actual force but quickly converges to the true value again. This overshoot is also due to the fast change in velocity, degrading the numerical differentiation.

VI. CONCLUSION

In this work, we introduce a framework to estimate contact force at the EE of an AM using only system state measurements without a direct force sensing device. We derive the dynamic model and the resulting expression for the external force at the EE. We validate the model in simulation in a scenario in which the AM establishes contact at the EE and eventually reaches a static equilibrium. Throughout the entire trajectory, including the flight, the impact, and static equilibrium, we estimate the contact force statically (i.e., assuming all derivatives are zero) and dynamically. Both resulting estimation methods can estimate the contact force precisely in the static equilibrium. Only the dynamic estimation, however, manages to estimate zero contact force during flight correctly and follow the transients during contact establishment.

In future work, this method for contact force estimation will enable a full-body, centralized controller that can enforce the desired system impedance. This implementation of variable impedance without a direct force sensor will enhance contact-based manipulation capabilities in AMs in the future. Further work also includes developing a physical prototype, which realizes the proposed estimation and a full-body control approach.
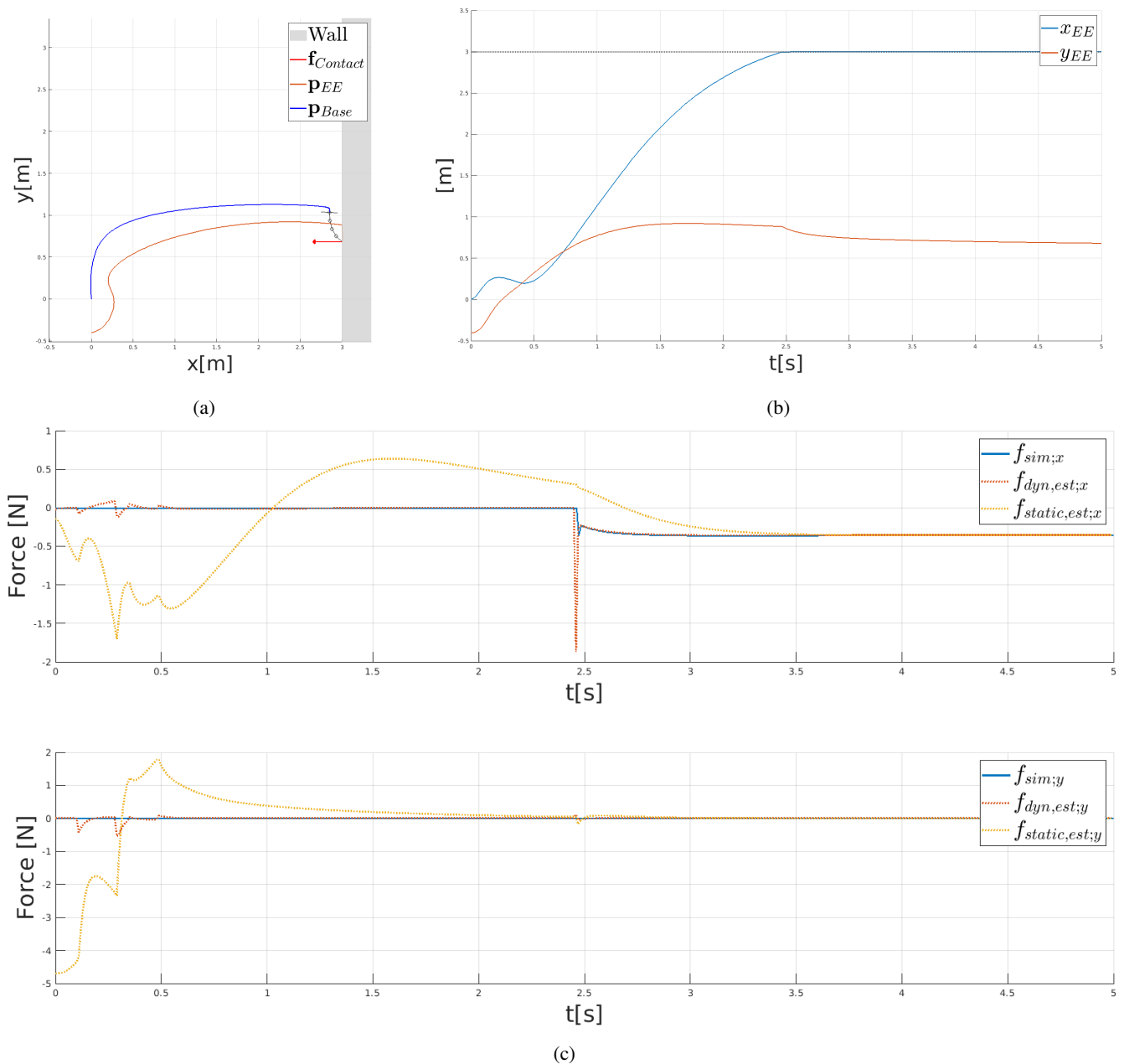
(a)

(b)

(c)

Fig. 4: Simulation results for the AM system. Top Left: the trajectory of the base and EE. Top right: the EE-coordinates over time. Bottom: the actual (blue) and estimated contact force (yellow: static, orange: dynamic). An animation of the path can be found at `https://youtube.com/playlist?list=PL6t4ON_jwwhGkzzlmkWlbkdg5tCMwThgL`.

REFERENCES

[1] A. Romero, S. Sun, P. Foehn, and D. Scaramuzza, "Model predictive contouring control for time-optimal quadrotor flight," *IEEE Transactions on Robotics*, pp. 1–17, 2022.

[2] M. Freeman, M. Kashani, and P. Vardanega, "Aerial robotic technologies for civil engineering: established and emerging practice," *Journal of Unmanned Vehicle Systems*, vol. 9, no. 2, pp. 75–91, 2021.

[3] S. Hamaza, I. Georgilas, M. Fernandez, P. Sanchez, T. Richardson, G. Heredia, and A. Ollero, "Sensor installation and retrieval operations using an unmanned aerial manipulator," *IEEE Robotics and Automation Letters*, vol. 4, no. 3, pp. 2793–2800, 2019.

[4] K. Bodie, M. Brunner, M. Pantic, S. Walser, P. Pfändler, U. Angst, R. Siegwart, and J. I. Nieto, "An omnidirectional aerial manipulation platform for contact-based inspection," *CoRR*, vol. abs/1905.03502, 2019.

[5] M. Tognon, H. A. T. Chávez, E. Gasparin, Q. Sablé, D. Bicego, A. Mallet, M. Lany, G. Santi, B. Revaz, J. Cortés, and A. Franchi, "A truly-redundant aerial manipulator system with application to push-and-slide inspection in industrial plants," *IEEE Robotics and Automation Letters*, vol. 4, no. 2, pp. 1846–1851, 2019.

[6] M. Mohammadi, D. Bicego, A. Franchi, D. Barcelli, and D. Prattichizzo, "Aerial tele-manipulation with passive tool via parallel position/force control," *Applied Sciences*, vol. 11, no. 19, p. 8955, 2021.

[7] L. Sciavicco and B. Siciliano, *Modelling and control of robot manipulators*. Springer Science & Business Media, 2001.

[8] E. H. Moore, "On the reciprocal of the general algebraic matrix," *Bull. Am. Math. Soc.*, vol. 26, pp. 394–395, 1920.

[9] Y.-F. Zheng and H. Hemami, "Mathematical modeling of a robot collision with its environment," *Journal of Robotic Systems*, vol. 2, pp. 289 – 307, 03 2007.